Comparison of outdoor and indoor PL and EL images in Si solar cells and panels for defect detection and classification

C. Terrados, D. González-Francés, V. Alonso, M.A. González, J. Jiménez, O. Martínez (*)

GdS-Optronlab group, Dpto. Física de la Materia Condensada, University of Valladolid, Valladolid, Spain

(*) oscar.martinez@uva.es

Keywords: electroluminescence, photoluminescence, solar cells, defect detection

Abstract

Nowadays, silicon solar plants consist of hundreds of thousands panels. The detection and characterization of the solar cell defects, particularly on-site, is crucial to keep a large productivity of the solar plant. Among the different techniques for the inspection of the solar cell defects, luminescence techniques give very useful information about the spatial distribution of defects. Actually, electroluminescence performed in dark conditions (nEL) is the most used technique. Recently, daylight EL (dEL) and daylight photoluminescence (dPL) have attracted interest, because they present noteworthy advantages for on-site inspections. In this paper, we present a detailed characterization, of both damaged mono- and multi- crystalline Silicon solar cells, using dEL and dPL, comparing the results provided by these techniques with those obtained with high resolution nEL and indoor PL (performed under excitation with a laser diode). Among these techniques, dEL provides reliable and reproducible results, while dPL shows a more dependence on the experimental conditions,

demanding an additional effort of comprehension. The limited resolution obtained with the actual IR camera technologies is a restraining factor of the dEL and dPL techniques. On the other hand, they can be performed on-site, testing a very large number of panels. Actually, we can assert that on-site dEL is well suited for massive inspection of solar plants, while more research is necessary for dPL

Introduction

Solar photovoltaics is now the most promising technology for renewable energy production [1-3]. Silicon solar plants consist of hundreds of thousands Si panels, a medium size PV plant (50 MW, with panels of 400 W) has more than 10^5 modules. The installed worldwide capacity in 2021 was 710 GW and is continuously growing [4]. The main element of the panel are the individual solar cells, obtained from bare Si wafers, conveniently doped to obtain the p-n junction, and with the necessary electrical contacts to collect the photogenerated carriers.

Defect characterization of the solar cells is a very important issue, with the aim to detect early failures and degradation of the Si solar panels [3]. For this purpose, several techniques are being used today –visual inspection, I-V characterization, infrared thermography (TIR), electroluminescence (EL), etc. –, being in general necessary a combination of some of them to understand the origin and the impact of the existing defects [5].

Taking into account the large number of solar panels installed nowadays, operation and maintenance (O&M) activities of large solar plants is mandatory, in order to keep the productivity, and to perform corrections on the degraded elements when necessary [6, 7]. Defect characterization of the Si solar cells is a crucial step of O&M [8].

Among the characterization techniques, the I-V curve gives characteristics (I_{sc}, V_{oc}, power, fill factor, etc.) of the module/string measured, with no indication of the localization of the possible defects. TIR gives spatial information about the defects, but the resolution of the TIR cameras is generally low and the images are usually obtained with a drone (at large distances), and the thermal signatures are difficult to assign to a specific type of defect. On the other hand, luminescence imaging provides a satisfactory spatial localization of the defects, allowing to identify different kinds of defects [7, 8]. The spatial resolution depends on the used sensor and the distance to the modules. Electroluminescence imaging (EL) is the most usually applied technique. The EL emission distribution provides detailed information about the semiconductor material and the electric contacts properties. The typical defects that can be detected are, at cell level: cracks and micro-cracks, wafer contaminations, soldering or ribbon interconnection failures, cell inhomogeneities, metallic finger interruptions and chemical corrosion (snail trails), while at module level: potential and light induced degradation (PID/LID), cell mismatch and short-circuited bypass diodes [9]. The main drawback of EL imaging, especially for inspections on-site, is the need for forward biasing the panels. On the other hand, traditionally the measurements have been done using a Si detector, for which inspections under strictly dark conditions are required (nEL), in order to avoid any background solar light [10]. The advantage of the Si detectors is their huge resolution (in terms of the density of pixels), allowing to have a very detailed image of the existing defects. In the last years, on-site EL (outdoor EL) has also been implemented, using different procedures to obtain a dark ambient [11, 12]. Moreover, more recently, also daylight EL (dEL) has been implemented. For this, an IR detector is mandatory (InGaAs cameras), as well as a procedure to suppress the background ambient light [10, 13, 14]. The measurement procedure consists, basically, of the subtraction of the signal collected by the detector when powering the PV panel, henceforth labeled as “on” state, and the signal collected without

powering the panel, “off” state. The main drawback of dEL compared to conventional nEL (on dark conditions using Si detectors), is the much lower resolution of the present IR cameras, because of the lower density of pixels.

Photoluminescence imaging (PL) is also useful to obtain information about defects in solar cells [15]. Traditionally, the need for a homogenous illumination source has prevented the use of PL imaging for the characterization of panels. However, with the apparition of dEL, also daylight PL (dPL) started to be implemented, using the sun light as the excitation source. As for dEL, a procedure for the suppression of the parasitic background light is necessary. This has been performed by measuring the PL signal in two different states of the solar panel, i.e. short circuit (off state) and open circuit (on state) conditions, being the dPL signal the difference between the two states [10, 16]. In open circuit conditions, the photogenerated carriers can recombine radiatively, producing a luminescence signal. In short circuit conditions, most of the photogenerated carriers escape through the electrical circuit and the luminescence signal is reduced. The difference between the two states allows to extract the PL signal, as described in ref. [16]. The procedure implies that the resultant dPL signal is also influenced by the electrical contacts; therefore, dPL cannot be assimilated to a PL measurement revealing the luminescence emission of the material. More recently, PL measurements have also started to be developed on-site, using a laser diode [17] or a LED [18] as the excitation source. In this case, no electrical contacts are needed, and the PL images reveal only the material defects.

In order to improve the comprehension of the dEL and dPL images obtained on-site, we performed a detailed comparison of the images acquired by nEL, dEL, dPL and PL excited by a laser diode (LD-PL), on both damaged mono-crystalline Si (m-Si) and multi-crystalline Si (mc-Si) solar cells. In particular, a discussion of the observed differences for dEL and dPL,

related to the differences in the measurement conditions, is presented here. The injection of carriers (dEL), and the extraction of carriers (dPL) are crucial for the image formation with both techniques. The detailed inspection of individual solar cells, with high resolution nEL and LD-PL images, and its comparison to dEL and dPL images, will provide a path to a better identification of the existing defects. The effects of the sensor resolution, the distance to the studied area, and the signal-to-noise ratio (SNR) on the image quality are also discussed.

Experimental and results

EL has been performed both indoor in dark conditions (nEL) as well as in daylight ambient (dEL) –using our self-developed technique for background light subtraction [10]– , using in both cases a power supply as the excitation source, Figure 1(a, b). Detailed nEL with the InGaAs camera has also been obtained for individual selected solar cells, both at 100% I_{sc} and 10% I_{sc}, since parallel resistance decreasing defects are properly detected at low injection, while series resistance increasing defects, such as inactive areas, are more easily detected at high carrier injection [18]. On the other hand, dPL with background subtraction [10] has also been performed, Figure 1(c). Besides, LD-PL was performed for individual selected solar cells using a laser diode (808 nm) as the excitation source, dispersing the laser light on each of the individual studied single cells, Figure 1(d). A multi-crystalline Si PV panel, with a large number of defects –not observable in a visual inspection–, as well as a large degraded (as revealed by simple visual inspection) mono-crystalline Si PV panel have been inspected. EL (both nEL and dEL) and dPL of the whole panels have been first obtained. Detailed nEL (at 100% I_{sc} and 10% I_{sc}) as well as LD-PL have been obtained subsequently for individual selected solar cells. In all cases the detection was done with an

InGaAs camera (Hamamatsu C12741-03) with 12.8 mm x 10.24 mm sensor size, and pixel size of 20 μm x 20 μm (thus with a total number of 640 x 512 pixels, i.e., 0,328 Mpixels). Additionally, nEL images of the whole panels obtained with a Si camera (Sony Alpha 7 III) with 35.5 mm x 23.8 mm sensor size, and pixel size of 0.7 μm x 0.7 μm (with a total number of 4240 x 2832 pixels, i.e., 12 MPixels) have also been obtained for comparison.

Multi-crystalline Si PV panel

A heavily damaged (27% power reduction from the nominal value – 255 W –, obtained from the I-V curve) mc-Si PV panel was first inspected using the four imaging techniques. Figure 2(a) shows the image obtained by a direct visual inspection, in which no defects were detectable. Figure 2(b-d) shows the corresponding nEL (b), dEL (c) and dPL (d) images of the whole PV panel obtained with the InGaAs camera, while Figure 2(e) shows the nEL image obtained with the Si camera. Obviously, the nEL image obtained with the Si camera gives an image better-defined than the one provided by the InGaAs camera. However, as mentioned, Si cameras do not allow for obtaining daylight luminescence images. Since dEL (and dPL) can be very valuable for a fast and massive panel inspection on-site, it would be useful to know their limitations, and capabilities, compared to nEL performed with Si cameras.

No significant differences between the nEL and dEL images obtained with the InGaAs camera are observed, despite the high irradiation conditions under which the dEL image was obtained (900 W/m^2). This demonstrates the capability of our subtracting method to obtain a high quality dEL image. On the other hand, the dPL image obtained under the same irradiation conditions (900 W/m^2) shows a different image pattern, as can be observed in more detail in Figure 3, where the zoomed nEL, dEL and dPL images of three selected

individual solar cells are shown. The selection of the cells has been performed according to their grey levels from the histogram, which can be supposed to be related to their level of damage, namely large, medium or small (labelled as #1, #2 and #3, respectively). These zoomed images evidence the lower resolution of the InGaAs camera. In fact, according to the detector dimensions and pixel sizes, the image of one solar cell (15.6 cm x 15.6 cm in this case) corresponds to approximately 425 x 425 pixels when the whole module is inspected with the Si camera, while only to approximately 64 x 64 pixels when the whole module is inspected with the InGaAs camera. For instance, thin isolated cracks are well visualized with the Si camera but are blurred when observed with the InGaAs camera [see the arrows in Figure 3 (b, e, k) and (c, f, l)].

As can be observed in Figure 3, the information provided by nEL and dEL images are essentially the same for the three solar cells, observing only a higher noise for the dEL images. The quantification of the noise has been performed by means of the SNR, as detailed below. On the other hand, the dPL image shows different features with respect to the EL images, except for the case of solar cell #3, for which the image pattern is nearly the same as for the EL images.

The noise level in the dEL and dPL images are due to the changes in the background light during the acquisition of the images [10, 19]. The noise can be reduced by acquiring a higher number of images (on/off cycles) (higher acquisition times). The SNR was evaluated according to the SNR_{avg} value described in ref. [19]. Figure 4 shows the dEL and dPL images of the whole mc-Si module under study, with the use of 100, 200 and 400 cycles in the case of dEL, while 200, 400 and 1000 cycles have been used in the case of dPL. The SNR_{avg} is found to increase with the number of on/off cycles, both for dEL and dPL images. On the other hand, SNR_{avg} is lower for dPL images with respect to the dEL images (comparing the

images obtained with the same number of cycles in each case), which is associated with the lower intensity of the luminescence signal in the dPL method compared to the dEL case, as will be discussed later on. According to ref. [19], a SNR_{avg} value of 5.0 is enough to have a good quality image. As observed, for dEL images this value can be reached with 200 cycles, while for dPL images the number of cycles must be significantly increased. Therefore, noise reduction can be achieved at the expense of increased acquisition time, a compromise between both is necessary.

Large spatial resolution can be obtained by bringing the camera close to the module. Figure 5 shows the dEL and dPL images obtained under the same irradiation conditions and using the same experimental parameters as those in Figure 4. The image quality is increased in this case (see for instance cell #1 in Fig. 5c, compared to Fig. 3d) due to the increased spatial resolution. The SNR_{avg} is increased by increasing the number of cycles. Moreover, the SNR_{avg} is a little higher now (Figure 5) respect to the previous situation (Figure 4) for the same number of on/off cycles, due to the closer position of the camera respect to the module, which implies a higher collection of photons.

A detailed inspection of the three selected cells of the mc-Si module was performed, in order to have a better understanding of the type of defects present in each cell. For this purpose, high resolution (HR) images with the InGaAs camera were obtained by centering the image on each of the selected cells. In particular, HR-nEL were obtained with the InGaAs camera, both at 10% I_{sc} and 100% I_{sc}, with the aim to distinguish between parallel and serial resistance defects. The resolution of the images in this case is highly improved, and can be as high that one solar cell (15.6 cm x 15.6 cm in this case) corresponds to 512 x 512 pixels, thus even improving the resolution obtained for one solar cell with the Si camera inspecting the whole module. Moreover, to distinguish the defects related to electrical contact failures from

bare defects related to material itself, we have excited each individual solar cell with a laser diode, thus obtaining also high-resolution LD-PL images.

Figure 6 (a-f) shows HR-nEL images obtained at 100% I_{sc} (a-c) and at 10% I_{sc} (d-f), and Figure 6 (g-i) shows the LD-PL images of the three solar cells. The main defects observed are: i) material inhomogeneities (typical in mc-Si), which are better revealed in the LD-PL (since for the EL image this information is lost in the areas where the failure of the electrical contacts is dominant), and ii) cracks and micro-cracks, which are critical to the module failure. Not all the cracks have the same impact, in fact the contrast in the images depends on the electrical connection to the other parts of the cell. One can classify cracks in three categories [20]: A) cracks, whose the surrounding areas are still electrically connected, and appear as thin, dark lines in the luminescence images; B) cracks, with areas partially connected to their surrounding regions through a finite resistance, the luminescence of the enclosed areas depends on the value of such resistance; and C) cracks, which are fully isolated from the rest of the cell, in this case the crack enclosed areas appear fully dark in EL images.

In LD-PL all the electrically connected cell parts would have roughly the same background PL intensity, which would be the case for areas separated by A and B cracks, while areas separated by C cracks are completely disconnected and their PL intensity can differ due to different recombination rates in the different cell parts [18].

If one compares the detailed information provided by the HR-EL and LD-PL images (Figure 6) with the low resolved dPL image (Figure 3), the information provided by the last one is not clear, it seems to be connected to the presence of C cracks. Moreover, as observed from different batches of dPL results (for instance those shown in Figures 4 and 5, compared to Fig. 2d), while the contrast in the dEL image depends only on the I_{sc} value, the dPL images

appear blind to some of the defects revealed in the EL images and the results depend more largely on the experimental conditions. In fact, dPL images are highly sensitive to the background light intensity, as the detection of some of the defects depends on the experimental conditions in terms of sun irradiation conditions. Cell #1 and #2 present dPL images with noteworthy differences with respect to the EL images, and largely depending on the experiment, while for cell #3 dPL reveals the same defects as that of EL. The essentially identical information provided by nEL, dEL and dPL in solar cell #3 can be related to cracks of type C, which represent regions of the cell fully electrically isolated.

The differences in the information provided by dEL and dPL should be ascribed to the different conditions of the measurements for each technique. Both of them are generated from a difference between two states and need of electrical contacts to be performed. In dEL, carriers are injected by the power source ("on" state), and the radiative recombination in the p-n junction gives a relative high luminescence signal, the "off" state (power off) being needed just to subtract the background solar radiation. In the case of dPL, the carriers are photogenerated and they recombine, the difference between the "on" state (open circuit) and "off" state (short circuit, in our case) permits to distinguish the luminescence emission from the ambient light (background). In dEL the injection of charge carriers guarantees the relatively high recombination in those areas where the p-n junction operates correctly, while in dPL the difference in the carrier populations available for recombination between the "on" and "off" state is the key factor. In dEL (as in nEL) a region will appear partially or totally dark if the area is electrically isolated (partially or totally) or there is a defect that produces a failure, total or partial, of the electrical contacts, e.g., cracks forming a loop. On the other hand, a complete electrically isolated area would appear dark in dPL images, because such area is not connected to the rest of the solar cell. Therefore, in dPL the open circuit and short circuit conditions are basically equivalents in terms of the light detected by the camera, thus,

the subtraction produces a dark image. Instead, for a partially electrically isolated area the subtraction of the "on" and "off" states in dPL would be different from zero because there is still a partial flow of carriers in short circuit, with the concomitant decrease of the photogenerated carriers for recombination. In fact, the differences between dEL and dPL should permit to establish the degree of isolation of different defects revealed in the images. However, additional tests are necessary to establish the optimum experimental conditions for the measurement of the dPL images.

Mono-crystalline Si PV panel

Figure 7(a) shows the visual image of a large damaged m-Si PV panel (43% power reduction from the nominal value – 175 W –, obtained from the I-V curve), where a high number of solar cells show delamination [6, 8]. Figure 7(b-d) shows the nEL, dEL and dPL of the entire PV panel obtained with the InGaAs camera, while Figure 7(e) shows the nEL image obtained with the Si camera. Four solar cells (their zoomed images are shown in Figure 8) have been selected in this case for a detailed analysis by means of HR-nEL and LD-PL characterization. with the use of the InGaAs camera.

Figure 9(a-h) shows the HR-nEL images obtained at high injection (a-d) and low injection (e-h) levels, while Figure 9(i-l) shows the LD-PL images for the four solar cells. The LD-PL as well as the HR-nEL images show clearly "tire wheel" defects for all the solar cells (which are ascribed to temperature inhomogeneities of the transport belt during the firing process to obtain the cells [9]), this information is lost in the low-resolution images of the whole panel obtained with the InGaAs camera. LD-PL images show also the presence of big cracks in solar cell #2, the delamination observed in solar cell #3, and the presence of thin lines corresponding also to A or B cracks in solar cell #4. This information is also observed in the

HR-nEL images, which emphasizes more clearly the electrical contact effects. However, the HR-nEL images of solar cell #1 at high injection reveals also problems in the fingers, thus ascribed to series resistance defects, which can be hardly detected by LD-PL.

Comparing the results with those obtained from the nEL, dEL and dPL images of the entire PV solar panel, it is clear that the small resolution of the InGaAs camera is a handicap. However, essentially the same information as that obtained from the HR-nEL images can be observed both in the nEL and dEL images. On the other hand, the dPL image provides also some useful information about areas with complete isolation (C crack defects), as is the case of solar cells #2 and #4.

As previously indicated, the image quality with the InGaAs camera is still a handicap with the present resolutions and the higher SNR compared to nEL. However, this could be overcome with the use of a large number of cycles and with the analysis of small regions. Daylight luminescence with InGaAs cameras, in particular dEL, is very well suited as an on-site inspection technique, giving very useful information of large defective areas of the modules.

Conclusions

HR-nEL and LD-PL allow to identify the main defects of m-Si and mc-Si solar cells. The comparison with daylight techniques, dEL and dPL, allow to get insight about the capabilities of the last ones for on-site characterization of the defects present in solar cells and solar panels, allowing the inspection of a large number of modules without dismounting them, and thus being very useful techniques for O&M activities. dEL needs for a power source and electrical contacts, while dPL under adequate irradiation conditions does not need for the power source; therefore, it significantly simplifies the operational inspection procedure.

However, dPL requires additional study, in order to assess the role of the background illumination, and the degree of isolation of the cracked regions, in the observation of defects and the image contrast. It appears that dPL reveals the areas with high electrical isolation, while dEL (which provides essentially the same information as nEL) supplies a much richer information about the contact fractures.

Acknowledgments

This work has been financed by the Spanish Ministry of Science and Innovation, under project PID2020-113533RB-C33 and by the Regional Government of Castilla y León (Junta de Castilla y León) and by the Ministry of Science and Innovation and the European Union NextGenerationEU / PRTR. C. Terrados also appreciates the funding from "Junta de Castilla y León" ("proyecto de garantía juvenil").

The authors declare that they have no conflict of interest.

References

[1] H. Bahar, P. Bojek, Solar PV. Tech. rep., Paris: International Energy Agency; 2020.

[2] Y. Chu, P. Meisen, Review and comparison of different solar energy technologies. San Diego, CA: Global Energy Network Institute (GENI); 2011.

[3] M. Kumar, A. Kumar, Performance assessment and degradation analysis of solar photovoltaic technologies: A review. Renew. Sustain. Energy Rev. 78, 554 (2017).

[4] https://www.statista.com/statistics/280220/global-cumulative-installed-solar-pv-capacity/

[5] S. Gallardo-Saavedra, L. Hernández-Callejo, M.C. Alonso-García, J.D. Santos, J.I. Morales-Aragones, V. Alonso-Gómez, A.M. Moretón-Fernández, M.A. González-Rebollo, O. Martínez. Nondestructive characterization of solar PV cells defects by means of electroluminescence, infrared thermography, I-V curves and visual tests: Experimental study and comparison. Energy 205, 117930 (2020).

[6] M. Aghaei, A. Fairbrother, A. Gok, S. Ahmad, S. Kazim, K. Lobato, G. Oreski, A. Reinders, J. Schmitz, M. Theelen, P. Yilmaz, J. Kettle, Review of degradation and failure phenomena in photovoltaic modules. Renew. Sustain. Energy Rev. 159, 112160 (2022).

[7] I. Høiaas, K. Grujic, A. Gerd, I. Burud, E. Olsen, N. Belbachir, Inspection and condition monitoring of large-scale photovoltaic power plants: A review of imaging technologies. Renew. Sustain. Energy Rev. 161, 112353 (2022).

[8] L. Koester, S. Lindig, A. Louwen, A. Astigarraga, G. Manzolini, D. Moser, Review of photovoltaic module degradation, field inspection techniques and techno-economic assessment. Renew. Sustain. Energy Rev. 165, 112616 (2022).

[9] M. Köntges, S. Kurtz, C. Packard, U. Jahn, K.A. Berger, K. Kato, T. Friesen, H Liu, et al. IEA-PVPS Task 13: Performance and Reliability of Photovoltaic Systems. Subtask 3.2: Review of Failures of Photovoltaic Modules. Technical report, International Energy Agency; 2014.

[10] M. Guada, A. Moretón, S. Rodríguez-Conde, L.A. Sánchez, M. Martínez, M.A. González, J. Jiménez, L. Pérez, V. Parra and O. Martínez (2020), Energy Science & Engineering 8, 3839 (2020).

[11] M. Navarrete, L. Pérez, F. Domínguez, G. Castillo, R. Gómez, M. Martínez, J. Coello, V. Parra, On-site inspection of PV modules using an internationally accredited PV mobile lab: A three-year experience operating worldwide, in 31st Eur. Photovolt. Sol. Energy Conf. Exhib. (2015), p. 1989.

[12] S. Koch, T. Weber, C. Sobottka, A. Fladung, P. Clemens, J. Berghold, Outdoor electroluminescence imaging of crystalline photovoltaic modules: comparative study between manual ground - level inspections and drone - based aerial surveys, in 32nd Eur. Photovolt. Sol. Energy Conf. Exhib. (2016), p. 1736.

[13] L. Stoicescu, M. Reuter, J.H. Werner, Daysy: luminescence imaging of PV modules in daylight, in 29th Eur. Photovolt. Sol. Energy Conf. Exhib. (2014), p. 2553.

[14] J. Adams, B. Doll, C. Buerhop, T. Pickel, J. Teubner, C. Camus, C.J. Brabec, Non-Stationary Outdoor EL-Measurements with a Fast and Highly Sensitive InGaAs Camera, in 32nd Eur. Photovolt. Sol. Energy Conf. Exhib. (2015), p. 1837.

[15] M. Demant, J. Haunschild, M. Glatthaar, M. Demant, J. Nievendick, M. Motzko, S. Rein, E.R. Weber, Quality control of as-cut multicrystalline silicon wafers using

photoluminescence imaging for solar cell production. Sol. Energy Mater. Sol. Cells. 94, 2007 (2010).

[16] R. Bhoopathy, O. Kunz, M. Juhl, T. Trupke, Z. Hameiri, Outdoor photoluminescence imaging of photovoltaic modules with sunlight excitation. Prog. Photovoltaics Res. Appl. 26, 69 (2018).

[17] G.A. dos Reis Benatto, C. Mantely, A.A. Santamaria Lancia, P.B. Poulsen, S. Forchhammery, S.V. Spataru, Laser Induced Luminescence Characterization of Mechanically Stressed PV Cells. Proceedings of 48th IEEE Photovoltaic Specialists Conference (2021), p. 1949.

[18] B. Doll, J. Hepp, M. Hoffmann, R. Schüler, C. Buerhop-Lutz, I.M. Peters, J.A. Hauch, A. Maier, C.J. Brabec, Photoluminescence for Defect Detection on Full-Sized Photovoltaic Modules. IEEE Journal of Photovolt. 11, 1419 (2021).

[19] C. Mantel, G.A. dos Reis Benatto, N. Riedel, S. Thorsteinsson, P.B. Poulsen, H. Parikh, S. Spataru, D. Sera and S. Forchhammer, SNR Study of Outdoor Electroluminescence Images under High Sun Irradiation, in 7th World Conference on Photovoltaic Energy Conversion (WCPEC) (2018), p. 3285.

[20] Köntges, M.; Kajari-Schröder, S.; Kunze, I.; Jahn, U. Crack Statistic of Crystalline Silicon Photovoltaic Modules. In Proceedings of the 26th Eur. Photovolt. Sol. Energy Conf. Exhib., Hamburg, Germany (2011), p. 3290.

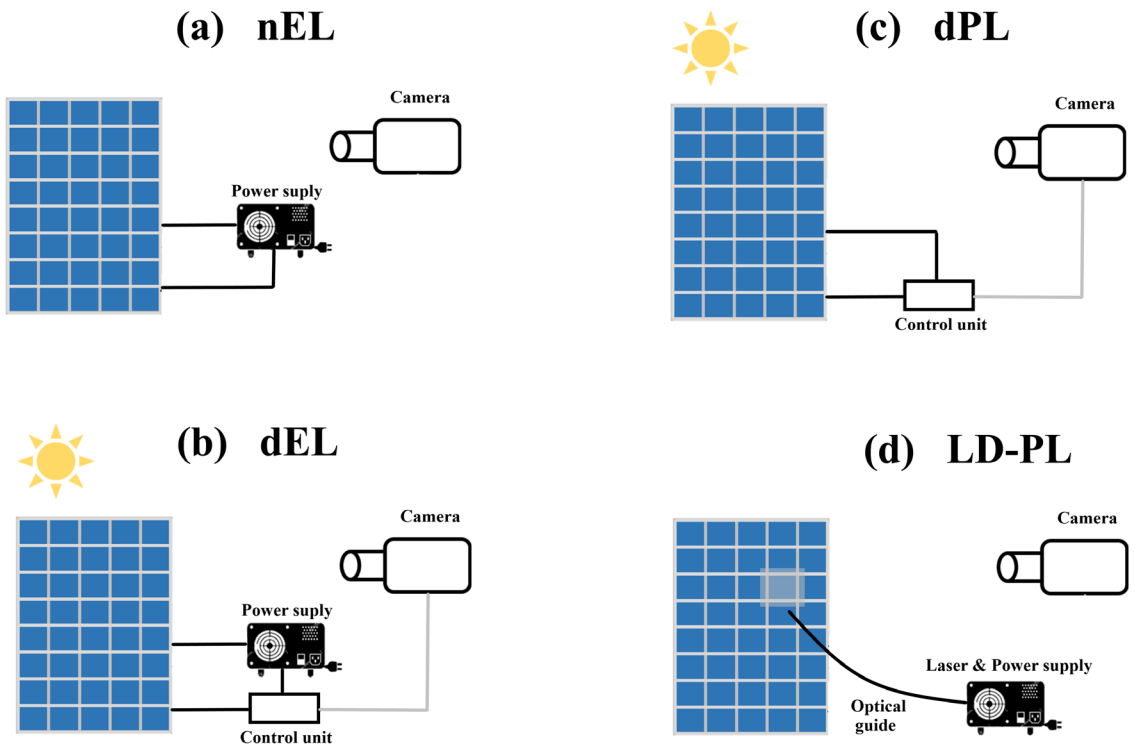

Fig. 1. Experimental set-up's for the four luminescence inspections techniques: (a) nEL set-up, for which a power supply is needed. The camera can be a Si or InGaAs sensor. (b) dEL set-up, obtained at any irradiation value; a control unit connected to both the power supply and the InGaAs camera is required for the on/off procedure. (c) dPL set-up, for which the power supply is not needed, only the control unit for the on/off procedure and the InGaAs camera are needed. (d) LD-PL set-up, with a laser diode that is dispersed on individual cells, and the InGaAs camera.

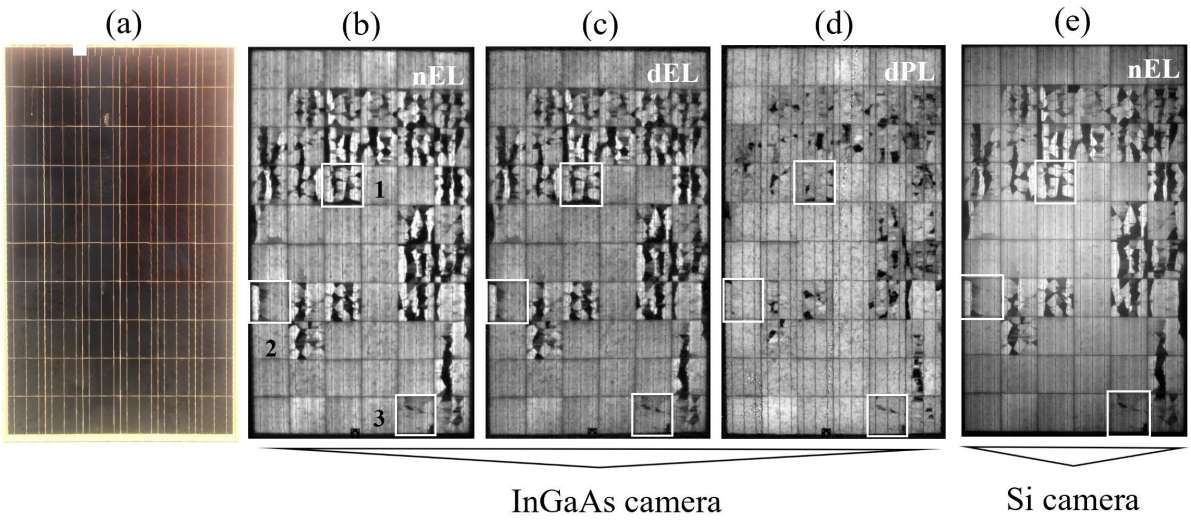

Fig. 2. (a) Visual image; (b) nEL image, (c) dEL image (obtained at 900 W/m^2), and (d) dPL image (obtained at 900 W/m^2), of a whole mc-Si PV panel obtained with the InGaAs camera; (e) nEL image of the whole mc-Si panel obtained with the Si camera. Three solar cells (marked on (b), and labelled as #1, #2 and #3) were selected for a detailed inspection

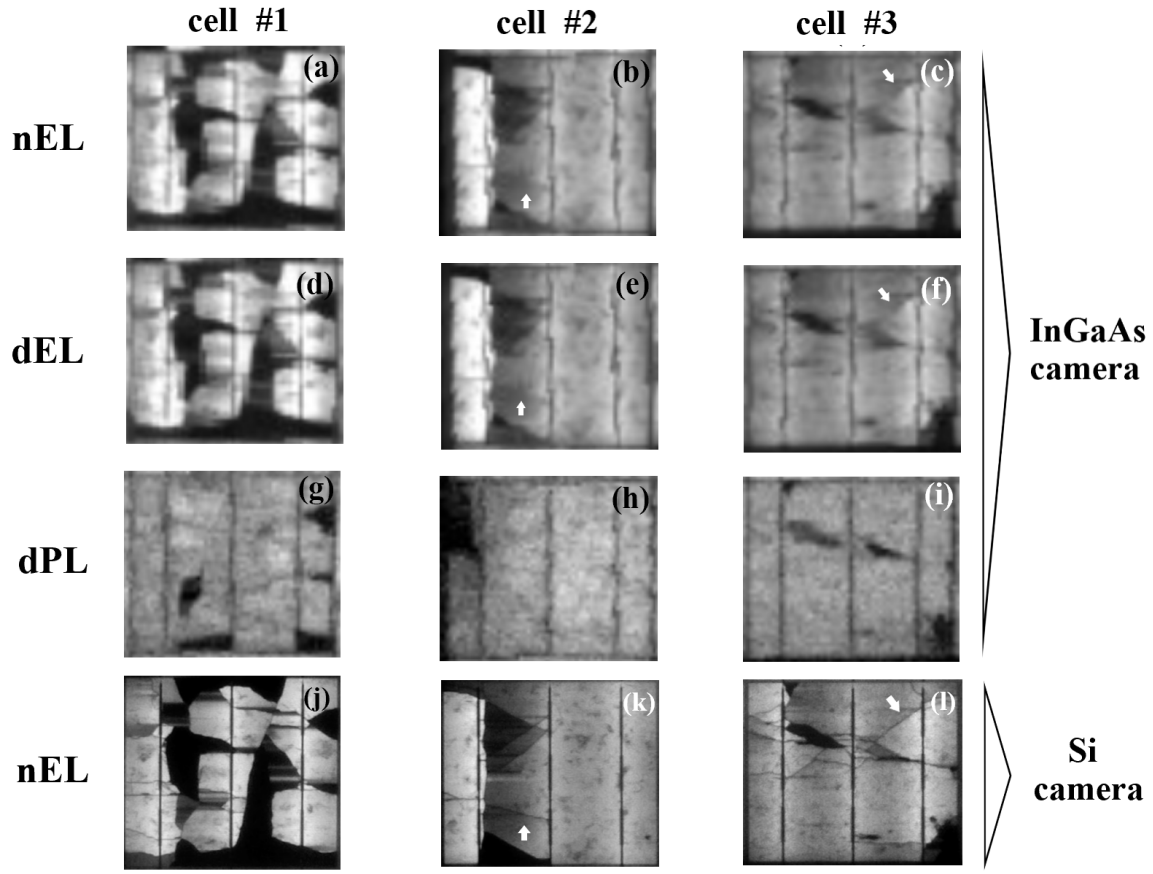

Fig. 3. Zoomed images of the three selected solar cells (mc-Si panel) marked on Fig. 2(b): (a-c) nEL images obtained with the InGaAs camera; (d-f) dEL images; (g-i) dPL images; (j-l) nEL images obtained with the Si camera. Isolated cracks observed with the Si camera (as those marked with arrows on (k) and (l)) are blurred when observed with the InGaAs camera due to its lower resolution [see arrows on (b,e) and (c,f)]

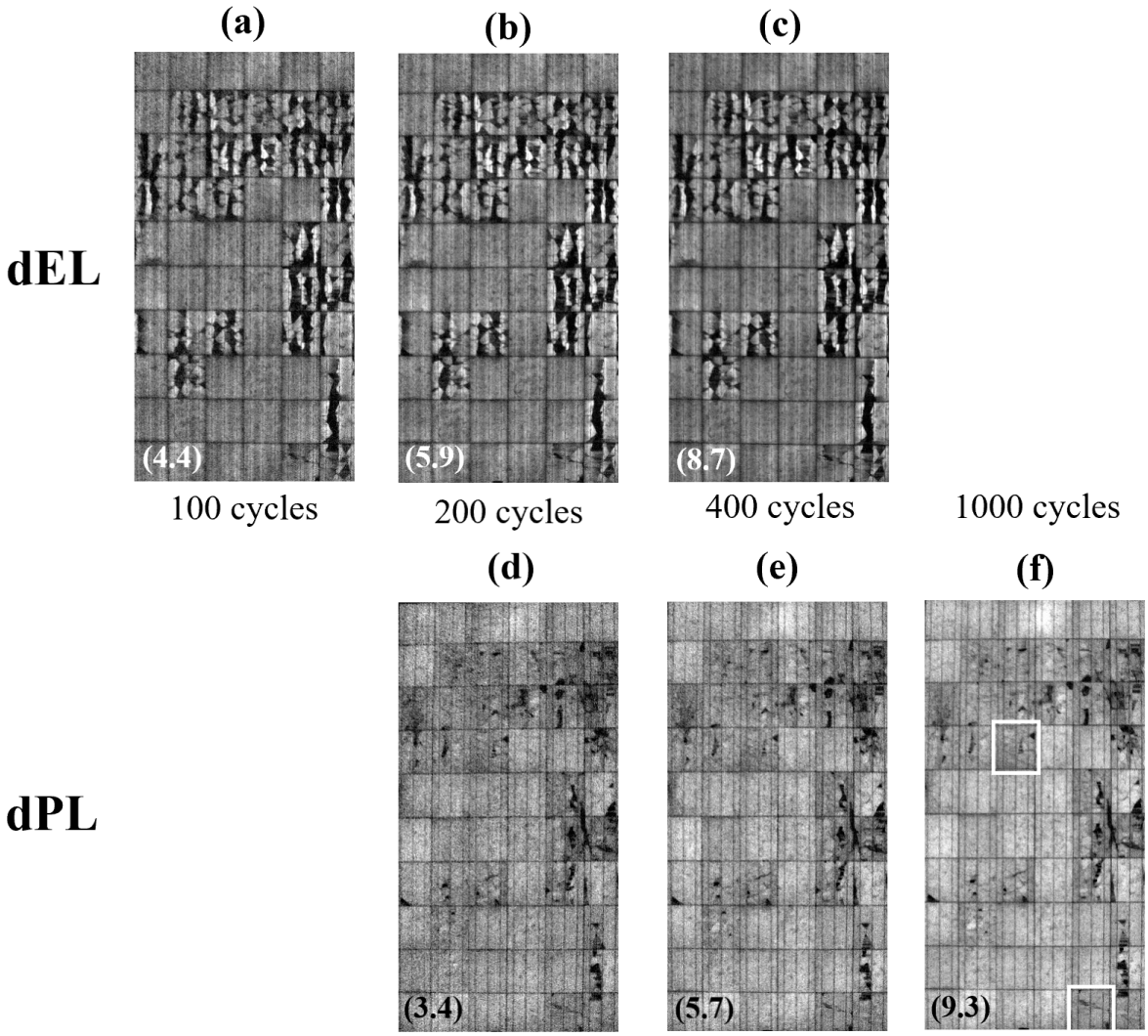

Fig. 4. dEL images (a, b, c) and dPL images (d, e, f) (at 900 W/m^2) of the whole mc-Si module obtained with (a) 100, (b, d) 200, (c, e) 400 and (f) 1000 on/off cycles. The values of the SNR_{avg} are given for each image (left corner, in brackets). Selected individual solar cells #1 and #3 are remarked on (f).

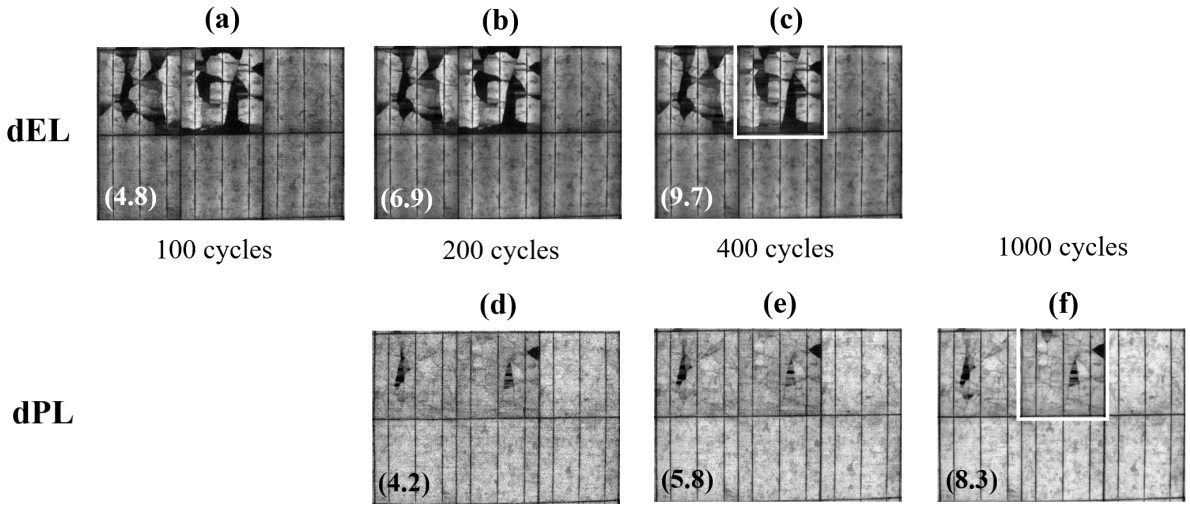

Fig. 5. dEL images (a, b, c) and dPL images (d, e. f) (at 900 W/m^2) of a smaller are of the mc-Si module shown in Fig. 4, obtained with (a) 100, (b, d) 200, (c, e) 400 and (f) 1000 on/off cycles. The values of the SNR_{avg} are given for each image (left corner, in brackets). Selected individual solar cell #1 is remarked on (c) and (f).

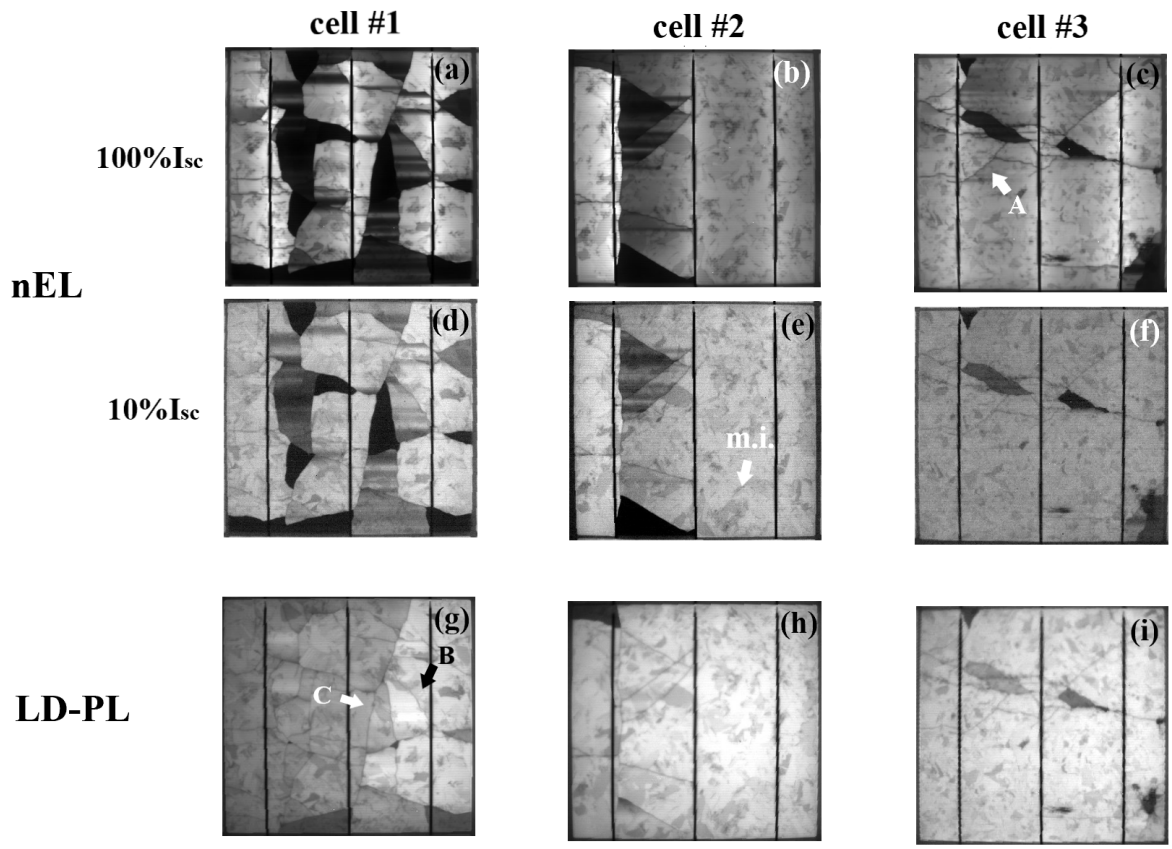

Fig. 6. Detailed inspection of the three selected solar cells (mc-Si panel) marked on Fig.1(b): (a-f) HR-nEL images at high injection (100% I_{sc}, a-c) and at low injection (10% I_{sc}, d-f); (g-i) LD-PL images (λ_{exc} = 808 nm, P_{exc} = 7 W) (m.i. ≡ material inhomogeneities; A, B, C ≡ cracks of type A, B or C)

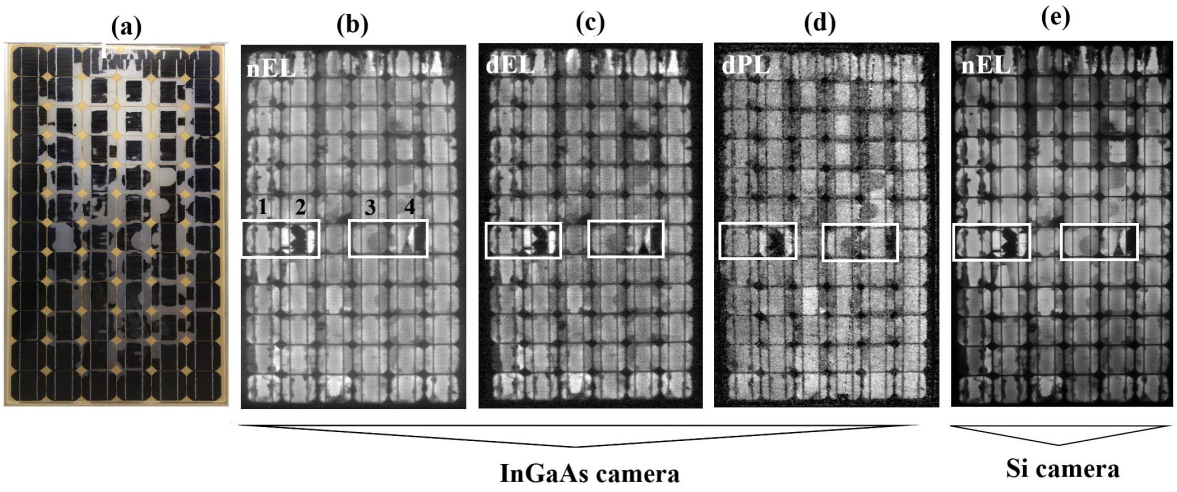

Figure 7. (a) Visual image; (b) nEL image, (c) dEL image (obtained at 900 W/m^2) and (d) dPL image (obtained at 900 W/m^2), of a whole m-Si PV panel obtained with the InGaAs camera; (e) nEL image obtained with the Si camera. Four solar cells (marked on (b), and labelled as #1, #2, #3 and #4) were selected for a detailed inspection

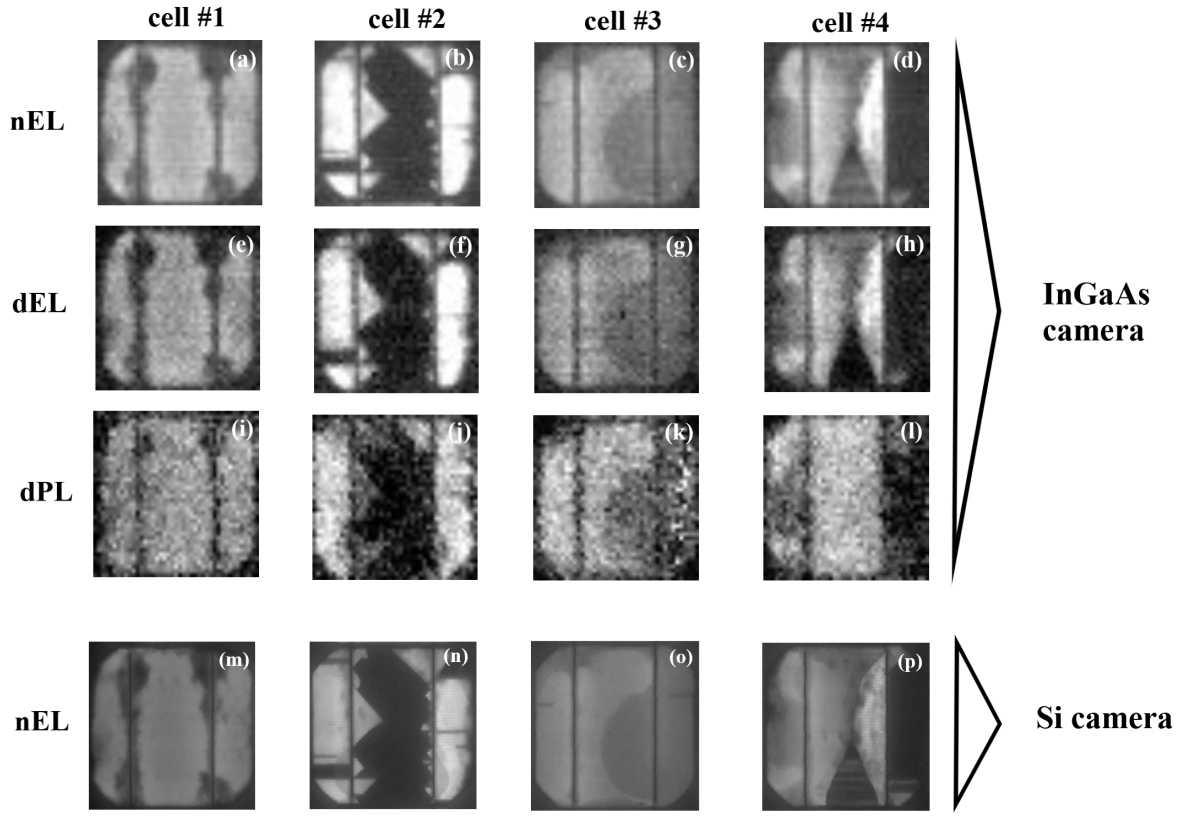

Fig. 8. Zoomed images of the four selected solar cells marked on Fig. 7(b): (a-d) nEL images, (e-h) dEL images, and (i-l) dPL images obtained with the InGaAs camera; (m-p) nEL images obtained with the Si camera

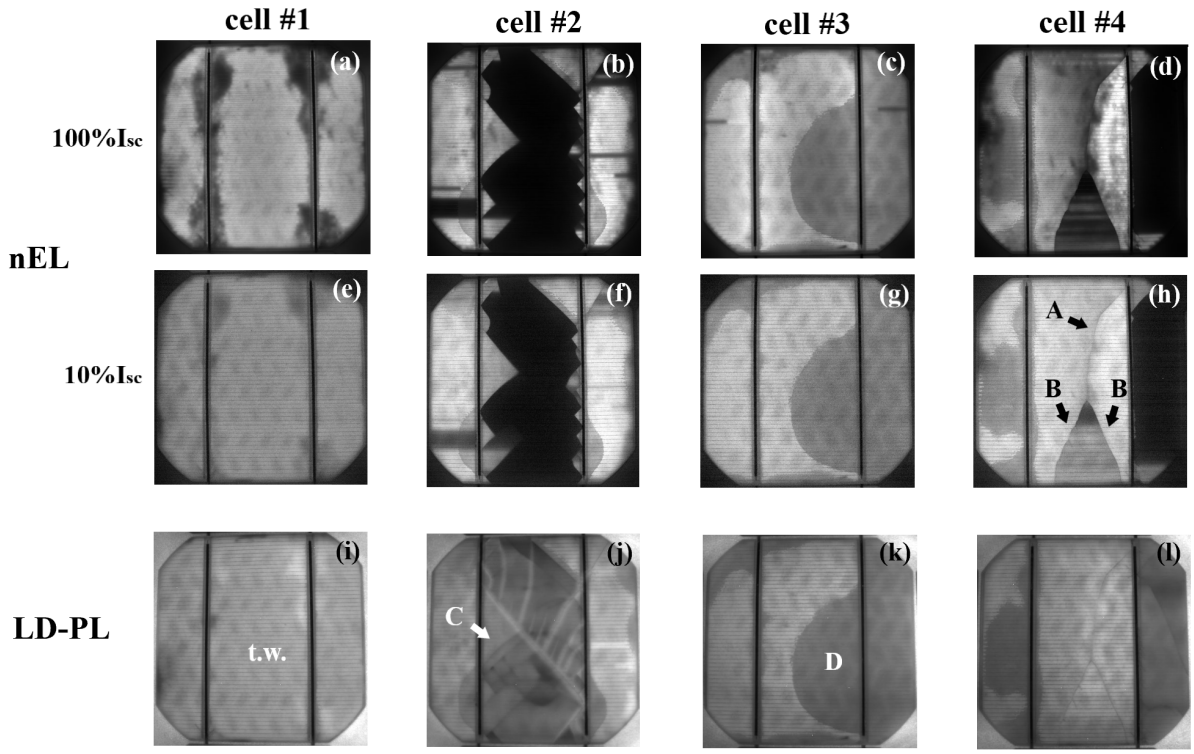

Fig. 9. Detailed inspection of the four selected solar cells marked on Fig.7(b): (a-h) HR-nEL images at high injection (100% I_{sc}, a-d), and at low injection (10% I_{sc}, e-h); (i-l) LD-PL images (t.w. ≡ "tire wheel" defects; A, B. C ≡ cracks of type A, B or C; D ≡ delamination)